JUNE 01 2001

# A theoretical study of passive control of duct noise using panels of varying compliance

Lixi Huang



*J. Acoust. Soc. Am.* 109, 2805–2814 (2001)
https://doi.org/10.1121/1.1369108



# A theoretical study of passive control of duct noise using panels of varying compliance

Lixi Huang
*Department of Mechanical Engineering, The Hong Kong Polytechnic University, Kowloon, Hong Kong*

(Received 8 June 1999; revised 25 October 2000; accepted 9 March 2001)

It is theoretically demonstrated that, in a duct, a substantial amount of sound energy can be transferred to flexural waves on a finite wall panel when the upstream portion of the panel is made to couple strongly with sound. The flexural wave then loses its energy either through radiating reflection sound waves or by internal friction. The effectiveness of the energy transfer and damping is greatly enhanced if the panel has a gradually decreasing *in vacuo* wave speed, which, in this study, is achieved by using a tapered membrane under tension. A high noise attenuation rate is possible with the usual viscoelastic materials such as rubber. The transmission loss has a broadband spectrum, and it offers an alternative to conventional duct lining where a smooth air passage is desired and nonacoustical considerations, such as chemical contamination or cost of operation maintenance, are important. Another advantage of the tapered panel is that, at very low frequencies, typically 5% of the first cut-on frequency of the duct, sound reflection occurs over the entire panel length. This supplements the inevitable drop in sound absorption coefficient, and a high transmission loss may still be obtained at very low frequencies.  [DOI: 10.1121/1.1369108]

PACS numbers: 43.50.Gf, 43.20.Mv, 43.20.Tb [MRS]

## I. INTRODUCTION

We are interested in devising a mechanism of broadband passive control of duct noise without using porous media such as glass wools or perforated metal sheets. Porous media have been the backbone of almost all dissipative noise abatement techniques (Beranek, 1992). When air is forced into the pores or cavities by sound, substantial viscous friction occurs between air and solid structures, typically fibrous and optimized to have the maximum surface contact area with air. The performance of a porous noise absorber is closely related to its ability to cause pressure loss to the mean flow. An air duct is often split into small channels with lined walls and the normalized flow resistance is usually over unity [Ingard (1994), p. 2-1]. If the flow speed is high, such lining may also cause extra noise. In addition, dusts get into pores easily and have to be cleaned periodically, which obviously contributes to the maintenance cost of building ventilation systems using porous linings. There are also places, such as operation theatres, where high hygienic requirement forbids the use of such materials. In fact, there are already public concerns of bacteria breading in the ventilation systems of ordinary commercial buildings equipped with central air conditioning systems. The use of porous material for noise or heat insulation purposes in the ventilation pipeworks is believed to contribute to an indoor air quality which is often worse than outdoors. The other problem of using porous or fibrous materials for sound absorption is that its performance degrades towards low frequencies, such as below 200 Hz.

To deal with the low-frequency noise and to avoid the disadvantages associated with the rough surfaces of porous materials, two types of membrane sound absorbers with smooth surfaces have been developed in the past. Ford and McCormick (1969) described an earlier type consisting of layers of thin membranes, such as 0.2 mm aluminum sheets, stacked at a certain distance from one another. They are used in broadcasting studios, concert halls, etc. Fuchs and his colleagues developed another type of membrane absorber (Ackermann *et al.*, 1988) in which a perforated thin plate is glued to an all-metal honeycomb structure forming an array of Helmholtz resonators. The device shows two resonance peaks relating to the Helmholtz resonance and the resonance of the cover plate, respectively. Another smooth cover sheet, typically of 0.1 mm aluminum, is then added in front of the perforated plate to protect the resonator from flow and dust. The separation distance is typically 1 mm. The result is an improved performance between the two resonance peaks. Membrane absorbers of this type has provided useful attenuation of low-frequency noise down to some 60 Hz when used in a papermill exhaust (Ackermann and Fuchs, 1989), but exact theoretical prediction proved rather difficult (Frommhold *et al.*, 1994). The main disadvantage of both types of membrane absorbers, however, is their narrow-bandedness typical of all resonator-type silencers. What is needed then is a nonresonator-type membrane absorber which will work for a broad frequency band. We propose to achieve this through transferring energy effectively from sound in air to the structural vibration by means of a strong fluid-structure coupling in the form of travelling waves.

The rationale behind introducing the strong air-structure coupling is that the attenuation of structural vibration could be made much higher than that resulted from the air-solid friction. Air-wall coupling has been a topic of investigation in the context of the so-called ''breakout noise'' from air-handling pipes (Cummings, 1994), but such coupling is unintended and the fraction of energy leaking is insignificant. If sound energy could be transferred to structure effectively, the expertise built in the field of vibration absorption and isolation will be readily deployed for noise absorption. The

question, then, is how could such energy transfer happen substantially and, if so, whether the damping coefficient required of the quick dissipation of structural energy is realistic? This study explores a theoretical model which yields encouraging answers to the above questions. The focus of this paper is on the characteristics of the fluid-structure coupling although the performance of such a potential noise absorption technique will also be briefly discussed. The present study is a development of the previous one on uniform panels (Huang, 1999), and the performance shown here represents a significant improvement in both sound reflection and dissipation.

We consider a finite, thin membrane under tension to form part of a duct wall. The panel has its own *in vacuo* wave speed, $c_T^*$, determined by its density and the tensile stress applied. Note that asterisk in the superscript signifies dimensional quantities which will be represented later by dimensionless ones of the same symbol without asterisk. The air-panel coupling is strong only when $c_T^*$ is close to the isentropic speed of sound in free space, $c_0^*$, which is around 340 m/s at room temperature. Under such a condition, the structure may be regarded as being 'transparent' to sound. But at such speed structural waves will go a long way without significant damping, which is undesirable for the purpose of noise absorption. So a gradation of $c_T^*$ is introduced to slow down the waves. We expect that the energy dissipation per unit distance will be increased to a level useful to noise absorption, which is confirmed in this study. We also found that the actual phase speed of the coupled wave, which is a function of the axial distance, $c^*(x^*)$, is somewhat less than $c_T^*$ due to air inertia, but $c^*(x^*)$ follows the trend of $c_T^*(x^*)$ rather closely.

As a preliminary study, we tactically make the following assumptions or exclusions, some of which may well be important in practical terms.

The frequency of the incident wave is below the first cut-on frequency of the duct.

Bending stiffness if ignored even though membranes of moderate to high thickness are implied in numerical examples. It is hoped that, in future studies, means other than using tapered membrane may be found to achieve a certain distribution of $c_T^*(x)$.

The problem of possible flow-induced vibration is potentially the most serious one and is left to future studies.

The effect of the fluid loading on the external side of the panel serves to complicate the algebra and is excluded.

The last assumption may need further justification. It is noted that when the external air is not confined, it exhibits evanescent waves with an effect of added mass. Therefore it is not expected to impact on the qualitative results sought in this study. In real applications, however, the external air may be confined by a solid wall to form a cavity to prevent noise breakout. The fluid loading inside the cavity is expected to play a similar role as that of the internal loading and, for the special case of a cavity having a depth equal to the main duct height, the total loading on the panel is simply double that of the present model without external fluid. The exclusion of the external fluid will be better appreciated when further details are revealed for the complicated cross-modal interactions and many other physical ingredients already present in the current model.

## II. FORMULATION OF NOISE-INDUCED VIBRATION

### A. The theoretical model

We consider an infinite channel of height $h^*$ fitted with a flexible strip of length $L^*$ on the lower channel wall. We call this strip a panel although the theoretical configuration is two-dimensional in nature. Noise of low frequency comes from the left-hand side of the channel and causes the panel to vibrate. We first limit ourselves to frequencies below the first cut-on frequency of the channel, $c_0^*/2h^*$. The questions we ask are what proportion of sound energy is reflected, how much is transmitted to downstream, and how much is damped by the internal friction of the panel? The reflection and absorption coefficients of energy are denoted by $\beta$ and $\alpha$, respectively, while TL represents the transmission loss.

All variables are normalized using the length scale $h^*$ and time scale $h^*/c_0^*$:

$$
\begin{aligned}
&x=\frac{x^*}{h^*}, \quad y=\frac{y^*}{h^*}, \quad t=\frac{c_0^* t^*}{h^*}, \quad c=\frac{c^*}{c_0^*},\\
&f=\frac{f^* h^*}{c_0^*}, \quad L=\frac{L^*}{h^*}, \quad k_0=\frac{\omega^* h^*}{c_0^*},\\
&\omega=2\pi\frac{f^*}{c_0^*/h^*}=k_0=2\pi f, \quad k=\frac{\omega}{c}, \quad \eta_0=\frac{\eta_0^*}{h^*}, \qquad (1)\\
&p=\frac{p^*}{\rho_0^*(c_0^*)^2}, \quad M=\frac{M^*}{\rho_0^* h^*}, \quad c_T=\frac{\sqrt{T^*/M^*}}{c_0^*},\\
&D=\frac{D^*}{\rho_0^* c_0^*}.
\end{aligned}
$$

The dimensionless symbols are explained below. $x$ and $y$ are the Cartesian coordinates. $L$ and $\eta_0$ are, respectively, the panel length and the amplitude of the local panel displacement. $c$ is the phase speed of the coupled wave in panel and air, which may differ from the isentropic speed of sound in free space, i.e., $c \neq 1$. $f$ is the dimensionless frequency, for which the first cut-on mode of a rigid wall duct has the value of 0.5. $k$ is the wave number based on $c$. The dimensionless angular frequency $\omega$ defined here is equivalent to the dimensionless wave number ($k_0$) based on the speed of sound in free space. $p$ is the general symbol for pressure perturbation. $c_T$ is the *in vacuo* wave speed provided by the tensile force $T^*$. The panel has a dimensional mass per unit area $M^*$ and damping $D^*$. The air has a mean density of $\rho_0^*$. $M$ and $D$ are, respectively, the dimensionless structure-to-air mass ratio (or simply mass henceforth) and the damping coefficient of the panel.

As shown in Fig. 1, the origin of the Cartesian coordinates, $x=y=0$, is located at the center of the panel which lies in the region of $|x|<L/2$. Both $M$ and $D$ may vary with $x$. The incident wave of unit amplitude is given as $p_i = \exp[i(\omega t - k_0 x)]$. The panel thickness distribution $b(x)$ is normalized by its mean, so that

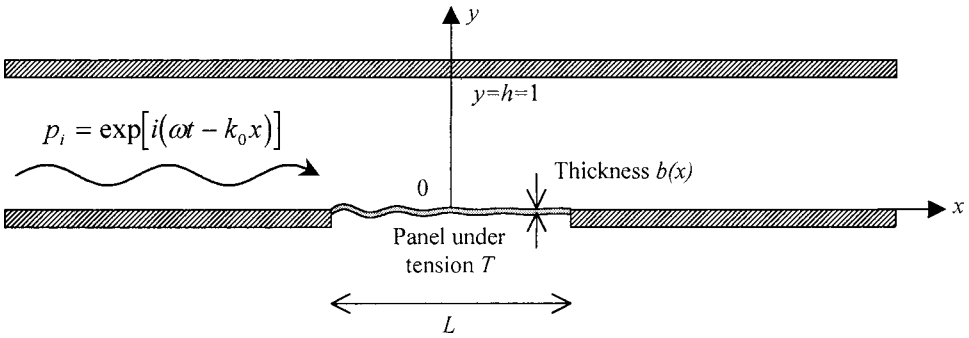


FIG. 1. The mathematical model of plane wave incident on a panel of nonuniform thickness. The panel has length $L$ and is under tensile force $T$. The thickness distribution function $b(x)$ is normalized to have a mean value of unity.

$$L^{-1}\int_{-L/2}^{+L/2} b(x)dx = 1.$$

The local panel mass is written as

$$M(x) = M_0 b(x),$$

where $M_0$ is the mass averaged over the whole length. The dynamics of the panel vibration is governed by

$$M(x)\frac{\partial^2 \eta}{\partial t^2} + D(x)\frac{\partial \eta}{\partial t} + p_w - T\frac{\partial^2 \eta}{\partial x^2} = 0, \tag{2}$$

where $p_w$ is the pressure perturbation on the inner side of the panel, the effect of fluid on the external surface being left to future studies as its inclusion at this moment may only serve to complicate the algebra. For instance, in real applications, the panel may be backed by an air cavity formed between the panel and a lower rigid wall to prevent the break-out noise. The cavity air pressure caused by the vibration of the panel is expected to have similar behavior to that inside the main duct. In the special case where the cavity has the same depth as the duct, the pressure loading $p_w$ is simply doubled. If the depth is different, the algebra will become rather involved. Therefore the present study is based on an idealistic model of no external fluid. The structural damping $D(x)$ is estimated by its *in vacuo* dynamics. By specifying $p_w = 0$ and $\eta = \eta_0 \exp[i(\omega t - kx)]$ we have

$$-M\omega^2 + Di\omega + Tk^2 = 0.$$

The loss factor of a material, $\sigma$, is defined as the ratio of energy damping per radian to the maximum potential energy [cf. Ungar (1997)]

$$\sigma = \frac{\frac{1}{2}D\omega|\eta_0^2|}{\frac{1}{2}(Tk^2)|\eta_0^2|} = \frac{D\omega}{Tk^2}.$$

The wave number $k$ here cannot be specified and for the tensioned membrane the issue of damping is in fact more complicated than that of bulk material (Berry, 1992). Since the present study is focused on other aspects of dynamics, we choose a simplistic model by substituting $k$ with $\omega/c_T$, so that

$$D = \frac{\sigma T k^2}{\omega}, \quad \frac{\sigma T\omega^2}{\omega c_T^2} = \sigma M\omega.$$

For metals, the loss factor $\sigma$ is in the range of $10^{-4}$ to $10^{-3}$ and is independent of frequency of the audio range. For viscoelastic materials like natural rubber, $\sigma$ is weakly dependent on frequency in the range of interest, such as from 100 Hz to 1 kHz. The value of $\sigma$ for the natural rubber at 100 Hz is 0.2 at room temperature. Damping for other viscoelastic materials can be over unity, and effective damping for composite structures like sandwiched or shearing layers can be even higher. The typical value we choose in our examples will be 0.05.

### B. Modal dynamics of the panel vibration

For harmonic excitation, the panel displacement may be replaced by its velocity as $\eta = V/i\omega$. Equation (2) may be rewritten as

$$\left(iM(x)\omega + D(x) - \frac{T}{i\omega}\frac{\partial^2}{\partial x^2}\right)V + p_w = 0. \tag{3}$$

In order to satisfy the structural boundary conditions of the panel, $V|_{x=\pm L/2} = 0$, we expand $V$ in terms of sine-transform using a local dimensionless variable $\xi = ((x/L) + \frac{1}{2})$ which spans from 0 to 1 for the panel:

$$V = \sum_{j=1}^{\infty} V_j \sin j\pi\xi, \quad V_j = 2\int_0^1 V(\xi)\sin j\pi\xi \, d\xi.$$

$V_j$ will be referred to as the coefficients of panel modes to avoid confusion with duct acoustic modes although $\sin j\pi\xi$ is certainly not the eigenfunctions of the tapered panel with or without fluid loading. The axial variations of the panel properties are expanded in terms of cosine-transform as follows:

$$M(x) = M_0\left(1 + \sum_{q=1}^{\infty} M_q \cos q\pi\xi\right),$$

$$D(x) = D_0\left(1 + \sum_{q=1}^{\infty} M_q \cos q\pi\xi\right),$$

where $D_0 = \sigma M_0\omega$. Multiplying Eq. (3) by $2\sin j\pi\xi$ and integrating over the panel length lead to

$$\int_0^1 \left[i\omega M(\xi) + D(\xi) + \frac{T}{i\omega}\left(\frac{j\pi}{L}\right)^2\right]V(\xi)2\sin j\pi\xi d\xi + p_{wj} = 0,$$

where

$$p_{wj} = \int_0^1 p_w 2\sin j\pi\xi \, d\xi.$$

Substituting $V(\xi)$ by its sine expansion and $M(\xi), D(\xi)$ by their cosine expansions, and defining

$$\mathcal{L}_j = i\omega M_0 + D + \frac{T}{i\omega}\left(\frac{j\pi}{L}\right)^2,$$
$$S_q = (i\omega M_0 + D_0) M_q, \quad j,q = 1,2,3,\ldots, \tag{4}$$

we get

$$\mathcal{L}_j V_j + \sum_{q=1}^{\infty}\sum_{j'=1}^{N} V_{j'} \int_0^1 2S_q[\cos q\pi\xi \sin j'\pi\xi \times \sin j\pi\xi]d\xi + p_{wj} = 0$$

in which

$$\int_0^1 [\cos q\pi\xi \sin j'\pi\xi \sin j\pi\xi]d\xi = \tfrac{1}{4}[\delta_{j'(j+q)} + \delta_{j'(j-q)} - \delta_{j'(q-j)}],$$

and $\delta_{ij}$ is the delta function. So that

$$\mathcal{L}_j V_j + \frac{1}{2}\sum_{q=1}^{\infty} S_q(V_{j+q} - V_{j-q} - V_{q-j}) + p_{wj} = 0, \quad j = 1,2,3,\ldots,N. \tag{5}$$

The $S_q$ series may be rewritten as

$$\sum_{q=1}^{\infty} S_q(V_{j+q} + V_{j-q} - V_{q-j}) = \sum_{n=1}^{N} Y_{jn}V_n, Y_{jn} = S_{n-j} + S_{j-n} - S_{j+n} \tag{6}$$

in which $S_{j\leqslant 0}$ should be assigned a value of zero.

The perturbation pressure on the wall ($p_w$) may be split into contributions from the incident wave and the radiation of its own. In terms of panel modes expansion,

$$p_{wj} = \sum_{n=1}^{N} V_n Z_{jn} + I_j, \tag{7}$$

where $Z_{jn}$ is the radiation impedance on the $j$th panel mode induced by the vibration of the $n$th mode, which has been calculated in a previous study (Huang, 1999) and the result is given below in terms of summations over duct acoustic modes,

$$Z_{jn} = 2\int_0^1 p_n \sin j\pi\xi \, d\xi = L\sum_{m=0}^{\infty} c_m(2-\delta_{0m})\mathcal{I}_2(m,n,j), \tag{8}$$

where $p_n$ is the radiation pressure of the $n$th mode, and

$$\mathcal{I}_2(m,n,j) = \frac{n\pi j\pi(e^{in\pi} - e^{-ik_mL})(e^{in\pi} + e^{ij\pi})}{[(k_mL)^2 - (n\pi)^2][(k_mL)^2 - (j\pi)^2]} - \frac{ik_mL\,\delta_{jn}}{(k_mL)^2 - (n\pi)^2}.$$

Here $c_m = [1-(m\pi/\omega)^2]^{-1/2}$ for cut-on modes, but $c_m = i|1-(m\pi/\omega)^2|^{-1/2}$ for cut-off modes, and $k_m = \omega/c_m$. Treatments for $\mathcal{I}_2$ (when it becomes 0/0-type) have also been given in (Huang, 1999). Note that it is necessary to take account of the cross-modal impedance, $z_{jn}$, $j \neq n$, since the panel dynamics are determined by the near-field pressure on the panel, which does not have the convenient orthogonal properties as far as the vibration modes are concerned.

$I_j$ is the sine-transform of the incident wave:

$$I_j = 2\int_0^1 e^{-ik_0L(\xi-1/2)}\sin(j\pi\xi)d\xi = 2j\pi e^{ik_0L/2}\left[\frac{e^{i(-k_0L+j\pi)}-1}{(k_0L)^2-(j\pi)^2}\right], \tag{9}$$

where the term in square brackets becomes $(2ik_0L)^{-1}$ when $k_0L \to j\pi$.

Inserting Eqs. (6) and (7) into Eq. (5) we have

$$\mathcal{L}_j V_j + \sum_{n=1}^{\infty} Y_{jn}V_n + \sum_{n=1}^{\infty} Z_{jn}V_n = -I_j, \quad j = 1,2,3,\ldots,N,$$

for which the solution is written in the following matrix form:

$$[V_j] = -\mathcal{Z}^{-1}[I_j], \quad \mathcal{Z} = [Z_{jn}] + [Y_{jn}] + [\mathcal{L}_{jj}].$$

Here $[V_j]$ and $[I_j]$ are column vectors, $[\mathcal{L}_{jj}]$ is a diagonal matrix formed by structural constants $\mathcal{L}_j$ defined in Eq. (4).

### C. Transmission loss and energetics of sound-panel coupling

The pressure perturbation induced by the wall oscillation was given by [Doak (1973), Eq. (123)] and is rewritten below in our notations and simplified for the two-dimensional configuration:

$$p(x,y,t) = \frac{1}{2}\sum_{m=0}^{\infty} c_m\psi_m(y)\int_{-L/2}^{+L/2}\psi_m(y')V(x',t) \times [H(x-x')e^{-i\omega(x-x')/c_m} + H(x'-x)e^{+i\omega(x-x')/c_m}]dx', \tag{10}$$

where $H$ is the Heaviside function, $y' = 0$ is the coordinate of the panel, $\psi_m$ is the channel modal function defined $\psi_m(y) = \sqrt{2-\delta_{0m}}\cos(m\pi y)$, and $c_m$ is the complex modal wave speed defined earlier.

The sound waves transmitted downstream is the sum of incident wave and the downstream travelling wave radiated by the vibrating panel. For excitation frequencies below that of the first cut-on frequency of the channel, sound waves radiated downstream, $x > L/2$, may be calculated from Eq. (10),

$$\frac{p_+}{p_i} = \frac{L}{2}\sum_{j=1}^{\infty} V_j\int_0^1 \sin(j\pi\xi')e^{ik_0L(\xi'-1/2)}\,d\xi' = \frac{L}{2}\sum_{j=1}^{\infty} V_j j\pi e^{-ik_0L/2}\left[\frac{e^{i(k_0L-j\pi)}-1}{(k_0L)^2-(j\pi)^2}\right],$$

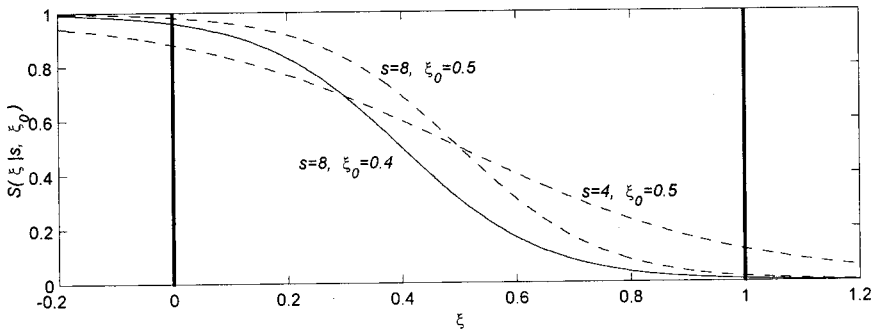


FIG. 2. Sigmoid curve used for *in vacuo* flexural wave speed prescription, $S(\xi|s,\xi_0)$, in which $s$ controls the steepness in the mid-range of $\xi$ and $\xi_0$ the center of symmetry. The solid curve with left-shift and moderately high steepness is the default shape used for later examples.

in which the square brackets takes the value of $i/2k_0L$ when $k_0L/\pi=j$. The transmission loss is found by

$$\mathrm{TL}=-20\log_{10}\left|\frac{p_i+p_+}{p_i}\right|.$$

Within the panel region, $|x|<L/2$, wave radiation from the panel is also split between left and right directions. The left-travelling wave is regarded as the local reflection wave,

$$p_-(x,t)=\frac{1}{2}e^{ik_0x}\int_x^{+L/2}V(x',t)e^{-ik_0x'}\,dx',$$

for which the time-mean intensity is calculated as

$$I_-\left(|x|<\frac{L}{2}\right)=\frac{1}{2}|p_-|^2=\frac{1}{8}\left|\int_x^{+L/2}V(x',t)e^{-ik_0x'}\,dx'\right|^2. \tag{11}$$

Once $I_-$ is calculated, the intensity of the right-travelling wave, $I_+$, can also be found by taking a control volume from $x=x$ to $x=L/2$ and writing the energy flux conservation as follows:

$$I_+(x)+\int_x^{L/2}I_s\,dx=I_-+I_{+\mathrm{TE}},$$

$$I_+(x)=I_{+\mathrm{TE}}+I_--\int_x^{L/2}I_s\,dx,$$

where subscript TE means evaluation at the trailing edge $x=L/2$. Here

$$I_s=\tfrac{1}{2}\mathrm{Re}[p_w\hat{V}] \tag{12}$$

is the sound radiation intensity from the panel, and $\hat{V}$ is the conjugate of $V$. The time-mean energy damping $I_d$ is found as

$$I_d=\tfrac{1}{2}\sigma M(x)\omega|V|^2 \tag{13}$$

and the energy balance between the incident, reflection, transmission waves and the damping is

$$\tfrac{1}{2}|p_i|^2=\tfrac{1}{2}|p_-|^2+\tfrac{1}{2}|p_i+p_+|^2+I_d,$$

which has been accurately validated in numerical implementations. Note that the reflection and damping coefficients are given by

$$\beta=\frac{|p_-|^2}{|p_i|^2},\quad \alpha=\frac{I_d}{\frac{1}{2}|p_i|^2}.$$

Also validated is the energy balance for the structure

$$\int_{-L/2}^{+L/2}(I_d+I_s)dx=0.$$

## III. ANALYSES OF RESULTS

We choose long panels of length $L=50$ with moderate damping as the default setting for the purpose of understanding wave behaviors, but the noise abatement performance of shorter panels ($L=10$) will also be discussed towards the end. Two identical panels are installed on the two channel walls, which is equivalent to having one panel in a channel of width $h^*/2$, a fact which is conveniently used in numerical calculations. The following parameters will be regarded as the default values in examples and will not be described again in figure captions or text,

$$L=50,\quad M_0=10,\quad \sigma=0.05.$$

Tapering of membrane thickness $b(x)$ is specified via the local *in vacuo* wave speed defined as $c_T(x)=\sqrt{T/M(x)}$ and a sigmoid curve defined as

$$S(\xi|s,\xi_0)=\frac{1}{1+e^{s(\xi-\xi_0)}},$$

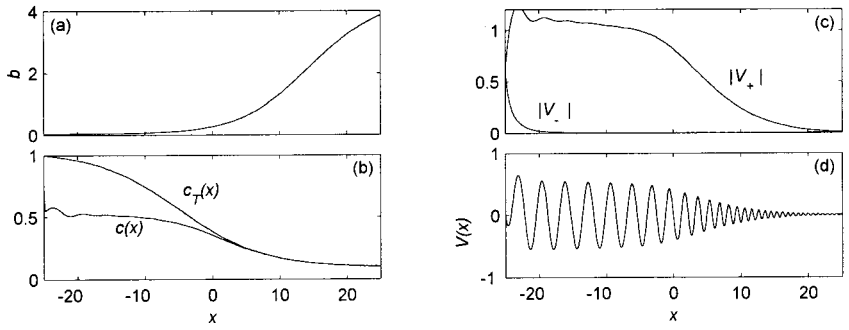


FIG. 3. The response of a tapered panel of default setting at frequency 0.15. $\alpha=0.095$, $\beta=0.905$, TL $=62.2$ dB.

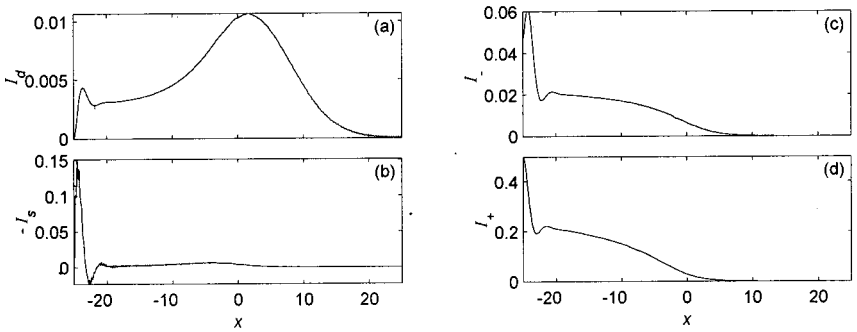


FIG. 4. Energetic analysis of the default tapered panel at frequency $f=0.15$. TL=62.2 dB.

$$c_T(\xi)=c_{T2}+\frac{S(\xi|s,\xi_0)-S(1|s,\xi_0)}{S(0|s,\xi_0)-S(1|s,\xi_0)}(c_{T1}-c_{T2}),$$

is adopted for easy manipulation of shapes as shown in Fig. 2. $c_{T1}$ and $c_{T2}$ are, respectively, the *in vacuo* wave speed at the upstream and downstream ends of the panel. The default values used in the calculations are

$$c_{T1}=1, \quad c_{T2}=0.1.$$

Parameter $s$ controls the curve steepness in the middle region, and $\xi_0$ is the center position of the curve which controls the relative slope at the leading and trailing edges. The larger $s$ is, the steeper the curve becomes in the middle region while the leading and trailing edges of the panel remain relatively smooth. Reducing $\xi_0$ has the effect of steepening the leading edge and flattening the trailing edge. The solid curve in Fig. 2 will be used as the default setting:

$$s=8, \quad \xi_0=0.4.$$

### A. Fluid-structure interaction

Figures 3 and 4 show the solution for the panel of default setting at frequency $f=0.15$. Figure 3(a) shows the tapering curve $b(x)$ which is essentially $c_T^{-1/2}(x)$. The mass ratio at the leading and trailing edges are 0.388 and 38.8, respectively. The flexural wave $e^{i\omega t}V(x)$ is decomposed into waves travelling to the left, $V_-$, and right, $V_+$, by means of

$$e^{i\omega t}\sin j\pi\xi=[e^{i(\omega t+j\pi\xi)}-e^{i(\omega t-j\pi\xi)}]/2i$$

and the results are shown in Fig. 3(c). The actual local wave speed is calculated as $c(x)=\omega/k(x)$, where $k(x)$ is the local gradient of decreasing phase angle of $V_+(x)$. The result is shown in Fig. 3(b). $c(x)$ follows $c_T(x)$ very well at the downstream half of the panel but the deviation is large at the upstream half. The reason is that the upstream half of the panel is thin and the fluid loading dominates. A snapshot of the vibration is shown in Fig. 3(d) confirming the shortening of the wavelength. The reduction of $|V_+(x)|$ in general is caused by both damping and sound radiation.

The reflection coefficient of sound energy ($\alpha$) is only 9.5% in this case, so the transmission loss of 62.2 dB is mainly contributed by the absorption in the form of flexural wave damping. The fact that the waves slow down should lead to a rising amplitude in $V_+$, but this is countered by the increase in panel mass and the removal of energy by damping. The full energy balance picture is shown in Fig. 4. Figure 4(a) gives the rate of energy damping per axial distance ($I_d$) defined by Eq. (13). The rate peaks somewhere in the middle of the panel due to the two competing factors. One is the increasing damping coefficient $D=\sigma M(x)\omega$, and the other is the decreasing vibration amplitude $|V(x)|$. Figure 4(b) gives the local energy influx from air to structure, $-I_s$, where $I_s$ is the sound radiation power defined in Eq. (12). The energy balance for the panel means that the integral of curves in Figs. 4(a) and (b) should be equal, which is confirmed in the calculation with a numerical error less than 0.015%. The spike in Fig. 4(b) means that the sound energy is transferred to the panel mainly near the leading edge but the damping by panel friction takes place rather gradually. Figure 4(c) shows the distribution of intensity of left-travelling sound, $I_-(x)$, and its axial gradient reflects the local contribution towards sound reflection by the tapered panel. Starting from the trailing edge, $I_-$ gathers strength and reaches about 0.02 near the leading edge, the slope being largest near the middle of the panel. Near the leading edge there is a distinct sharp rise in $I_-$ representing the effect of scattering of incident wave. At $x=-L/2$, $I_-=0.047$ is the intensity of reflection sound further upstream which is somewhat lower than the peak of $I_-(x)$, indicating a destructive interference of reflection waves radiated over the panel length and the scattering by the leading edge. Figure 4(d) gives the intensity of the right-travelling sound, $I_+(x)$, which is the sum of the incident sound $p_i$ and the panel radiation. The sharpest reduction of $I_+$ occurs near the leading edge where two events occur: (a) wave scattering by the leading edge, and (b) energy tansfer from sound to the panel, the latter being dominant in this case.

### B. Comparison with uniform panel

We now compare the behavior of the typical tapered panel with that of a uniform panel and the results are listed in Table I. The uniform panel has the same mass of $M=10$, a damping coefficient of $\sigma=0.05$, and a tension of $T=0.39$ corresponding to the value of the *in vacuo* wave speed of

TABLE I. Comparison of tapered and uniform panels.

| Panel | Tapered | Uniform | Tapered | Uniform |
|---|---|---|---|---|
| $f$ | 0.15 | 0.15 | 0.05 | 0.05 |
| $c_T$ | 1→0.1 | 0.20 | 1→0.1 | 0.20 |
| $c$ | 0.52→0.1 | 1.14 | 0.34→0.1 | 0.19 |
| Reflection $\beta$ (%) | 9.5 | 0.3 | 20.2 | 44.1 |
| Absorption $\alpha$ (%) | 90.5 | 49.4 | 79.5 | 55.0 |
| TL (dB) | 62.2 | 3.0 | 25.0 | 20.5 |

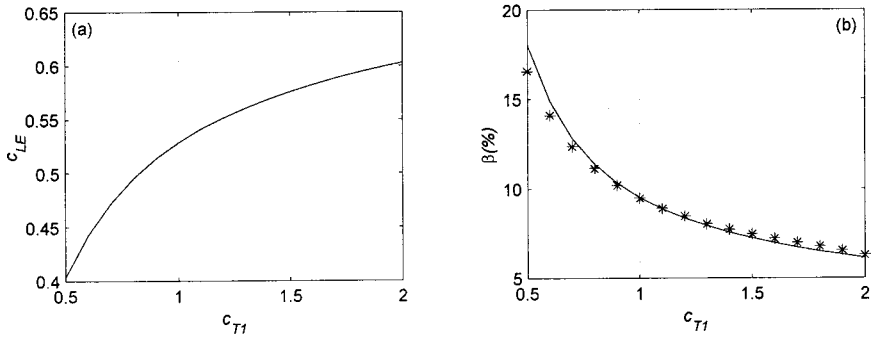


FIG. 5. Interface model for sound reflection. The panel parameters are those of default except $c_{T1}$. The frequency is 0.15. (a) is the variation of prevailing wave speed near the leading edge against $c_{T1}$, and (b) shows the agreement between the actual sound reflection coefficient $\beta$ (shown as $*$) and that predicted by the interface model $R_{\text{int}}$ (shown as the solid line).

$c_T=0.2$ We first calculate for the frequency of $f=0.15$ for which the results are listed at the second and third columns of Table I. For the tapered panel, the actual wave speed $c(x)$ varies from 0.52 at the leading edge towards 0.1 at the trailing edge, but for the uniform panel, the subsonic wave is dominated by the supersonic wave of speed 1.14; supersonic eigenvalue being identified in the previous study (Huang, 1999). Since the wave speed is very close to unity, very little reflection occurs. Damping takes away 49.4% of the sound energy, which is much lower than 90.5% on the tapered panel. This clearly demonstrates the utility of panel tapering. We then test a lower frequency of $f=0.05$ at which supersonic wave is avoided in the uniform panel. The results are shown at the last two columns of Table I. It is found that the tapered panel has a higher wave speed near the leading edge and the reflection is much lower than that of the uniform panel. But the much improved damping compensates for the overall performance in transmission loss. In fact the tapered panel has a TL of 25.0 dB while the uniform panel has 20.5 dB.

### C. Modelling of the sound reflection

When using tapered panels, one wishes to maximize sound absorption coefficient $\alpha$, but absorption cannot occur for sound reflected at the leading edge of the panel. In this section, we attempt to model the sound reflection coefficient $\beta$ so that ways may be found to minimize it. As shown in the typical case of Fig. 3(b), the actual wave speed $c(x)$ is rather constant at the first one third of the panel length where the intensity of the upstream travelling sound, $I_-$, is significant. We model the sound reflection by the panel by replacing the panel with a hard wall and filling the whole downstream duct with another fluid with the density of air but a speed of sound equivalent to the prevailing flexural wave speed at the upstream portion of the panel denoted as $c_{\text{LE}}$. $c_{\text{LE}}$ may be calculated by averaging the phase speed $c(x)$ over the first 25% of the panel length. For example, for the basic case shown in Fig. 3(b), $c_{\text{LE}}$ is found to be 0.52. We call this interface model. The panel is finite but the damping used in the default setting is expected to eliminate substantial flexural wave reflection at the trailing edge, which provides some ground for optimism for the interface model. The reflection at such interface is

$$R_{\text{int}}=\left(\frac{1-c_{\text{LE}}}{1+c_{\text{LE}}}\right)^2.$$

For the default panel setting, $c_{\text{LE}}=0.52$ and $R_{\text{int}}=10.0\%$, comparing well with the actual result of $\beta=9.5\%$. We now vary the panel property by changing $c_{T1}$ from 0.5 to 2.0 in order to change $c_{\text{LE}}$ to validate the interface model. The result is shown in Fig. 5, which shows good agreement. Should $c_{\text{LE}}$ reach unity, sound reflection might be eliminated.

Having identified the deviation of $c_{\text{LE}}$ from unity [as shown in Fig. 5(a)] as the main source of sound reflection, we now focus on why $c_{\text{LE}}<c_{T1}$. The reason is that the air imposes virtual mass on the panel. For waves travelling to the right at constant speed $c$, the virtual mass may be found as

$$m_a=\frac{p}{i\omega V}=\frac{\coth k_a}{k_a},\quad k_a=\sqrt{\left(\frac{\omega}{c}\right)^2-\left(\frac{\omega}{c_0}\right)^2}$$

(Huang, 1999). When $c\to c_0=1$, $k_a\to 0$, $m_a\to\infty$. For $c<1$, lower frequency gives lower $k_a$, hence higher virtual mass. As $\omega\to 0$, $k_a\to 0$, $m_a\to\infty$, whatever the wave speed $c$. This analysis does not account for the fact that, near the leading edge, the panel experiences standing flexural waves,

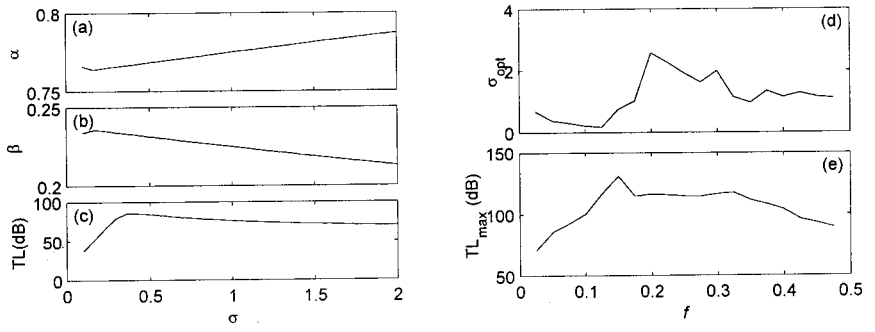


FIG. 6. Effect of damping parameter $\sigma$. (a) gives the sound absorption coefficient $\alpha$, (b) gives the reflection coefficient $\beta$, and (c) shows the corresponding TL. All are calculated for $f=0.15$. (d) and (e) are the optimal damping coefficient $\sigma$ and maximum TL, determined by the peak in (c), as a function of frequency.

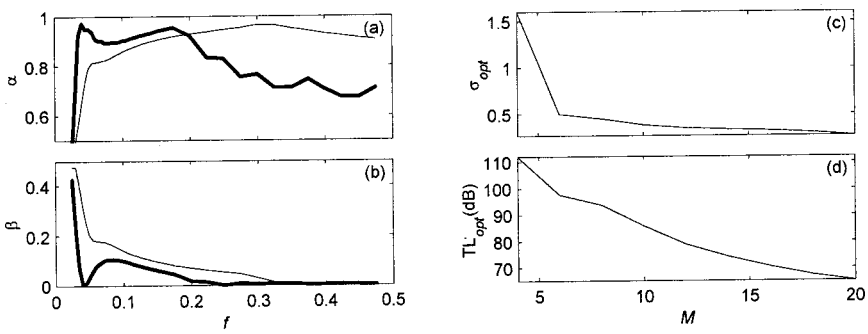


FIG. 7. Effect of mass on spectral performance and optimal damping. For (a) and (b) the thin solid lines are for the default panel of $M=10$, $\sigma=0.05$ while the thick one is for the heavy panel of $M=30$, $\sigma=0.05/3$. The loss factor $\sigma$ is reduced so that the effective energy damping determined by $M\sigma$ is the same. For (c) and (d) the frequency is 0.05.

but the virtual mass factor could play an important role, especially where the panel is thin.

### D. Optimal damping

For the moderate frequency of $f=0.15$, the variations of sound absorption and reflection coefficients with the material loss factor $\sigma$ are shown in Figs. 6(a), (b), and (c) for the default panel setting. Damping reduces reflection $\beta$ and increases absorption $\alpha$ over almost the whole range of $\sigma$ shown above, but the total transmission loss has a peak at $\sigma=0.38$. The variation of the optimal loss factor ($\sigma_{\text{opt}}$) with frequency is shown in Fig. 6(d). Note that, for short panels, the curve of this relationship exhibits a highly oscillatory behavior. The maximum transmission loss achieved with the optimal loss factor is shown in Fig. 6(e).

### E. The effects of mass and tension

The variation with panel mass $M$ is studied by raising $M$ while keeping $M\sigma$ constant since the latter determines the damping coefficient $D$. The results are shown in Figs. 7(a) and (b) covering the whole frequency range. The thick lines are for the heavier panel which has $M=30$. The heavier panel has less sound reflection over the whole frequency range. The reason is that the virtual mass that air imposes on the vibrating panel is relatively small and, as a result, the actual wave speed near the leading edge, $c_{\text{LE}}$, is closer to its *in vacuo* value $c_{T1}$. The absorption coefficient $\alpha$ increaseas at frequencies less than about 0.2 in the example but decreases at higher frequencies. The increase is related to the reduction in sound reflection but the decrease is associated with the lack of response from heavier panels at high frequencies. In Figs. 7(c) and (d) the effect of mass on the optimal loss factor $\sigma_{\text{opt}}$ and the corresponding optimal transmission loss $TL_{\text{opt}}$ are presented for the frequency of 0.05. The conclusion is that heavy panels cannot take advantage of higher damping.

The effects of tension are studied by increasing or decreasing the values of $c_{T1}$ and $c_{\text{T2}}$ proportionally so that the shape of $c_T(x)$ remains unchanged. Panels with higher tension are represented by thinner lines in Fig. 8. The thinnest line is for the case of $T=1.55$, $c_{T1}=2$, $c_{T2}=0.2$, while the thickest line is for the case of $T=0.097$, $c_{T1}=0.5$, $c_{T2}=0.05$. When the tension is increased, sound reflection reduces and absorption increases, although at very low frequency range there are considerable spectral oscillation, as expected. For panels with higher $c_{T1}$, the actual $c_{\text{LE}}$ is closer to unity, hence less reflection. Notice that the increase in $c_{T2}$ and $c_T(x)$ in general should not favor wave absorption, given the same amount of incident flexural waves, but the absorption coefficient is increased for panels with higher tension in this case. The reason is that the damping coefficient chosen for the default panel is high enough to absorb the increased amount of energy in the excited flexural waves.

### F. Frictionless panels

Now we discuss cases where the finiteness of the panel plays an important role in sound reflection by considering frictionless panels. We first consider short panels of length $L=10$, and the distributions of left-travelling sound intensity, $I_-(x)$, are shown in Figs. 9(a) and (b). Figure 9(a) is for the frequency of $f=0.05$ and Figure 9(b) is for the frequency of 0.06. The oscillatory pattern of $I_-(x)$ is indicative of interference of sound waves reflected from different parts of the tapered panel. In the case of Fig. 9(a), the total intensity of the reflected sound at the leading edge is at the peak of the variation pattern, and $\beta$ is 96.5%. In the case of Fig. 9(b), however, one can see values of $I_-$ in excess of 0.5 (i.e.,

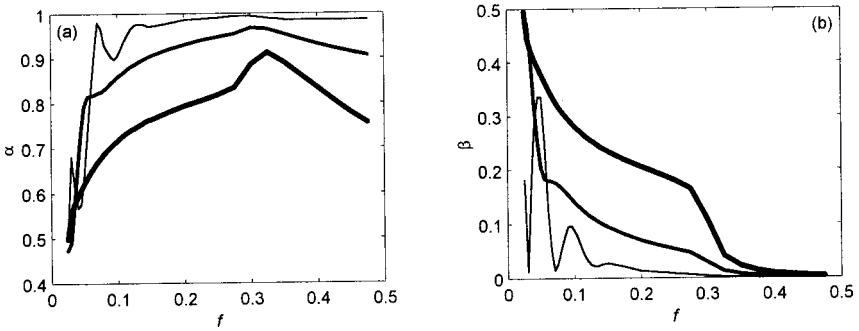


FIG. 8. Effect of tension on sound absorption coefficient $\alpha$ and reflection coefficient $\beta$. The panel properties are those of default except the thin line has tension four times the default value of $T=0.39$ (medium thickness line) while the thickest line has a quarter of the default tension.

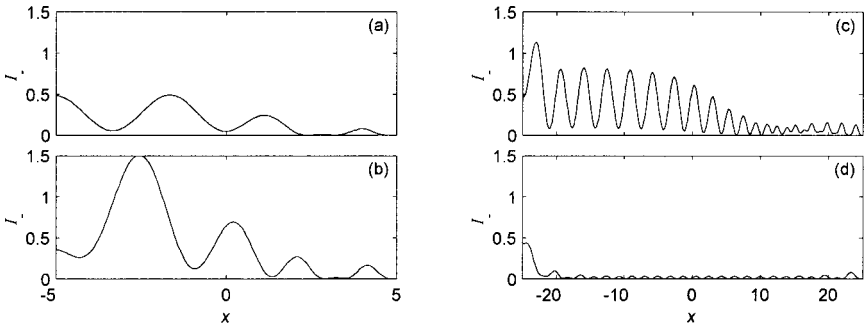


FIG. 9. Distributions of intensity of upstream travelling sound. The four cases are (a) $L=10$, $f=0.05$, $\beta=96.5\%$, (b) $L=10$, $f=0.06$, $\beta=71.0\%$, (c) $L=50$, $f=0.05$, $\beta=92.5\%$, (d) $L=50$, $f=0.05$, uniform panel of the same tension ($T=0.39$), $\beta=85.2\%$.

$\beta=1$) locally, but the total reflection is only 71.0% as the leading edge emerges near the bottom of the interference pattern. Figures 9(c) and (d) are for the default panel length of 50 and the frequencies are both 0.05. Figure 9(c) is for the tapered panel while Fig. 9(d) is for the uniform panel subject to the same tension as the tapered panel. The tapered panel has 92.5% sound reflection but the uniform panel has only 85.2%. The axial variation of $I_-(x)$ again suggests constructive and destructive interference of the reflection waves on the tapered panel. The lack of such varitaion on the uniform panel indicates that there is little reflection except around the leading edge. The prevailing wave speed near the leading edge ($c_{LE}$) is 0.33, 0.30, 0.33, and 0.52 for the four cases, and the corresponding reflection coefficients according to the interface model are 25%, 29%, 25%, 10%, respectively. The actual reflection in these cases are all much higher. This is because, on a frictionless panel, there is strong reflection of flexural waves by the trailing edge, $V_-(x)$, which radiates sound upstream very effectively.

The variation of wave reflection with the panel length is given in Fig. 10 for the frequency of $f=0.15$. The thick solid line is for the tapered panel, which shows a persistent performance when used as a noise reflector. The other two lines are for uniform panels with the same *in vacuo* wave speed of $c_T=0.20$, the solid line is for mass $M=10$, which is the same as the tapered panel, while the dashed line is for a light panel of $M=1$. The heavy uniform panel hardly reflects any sound except at a few discrete points, which is why we introduce the light one for comparison. The reflection is higher on the light uniform panel but passbands exist, which is typical of conventional reactive mufflers.

### G. Performance of panel muffler

For the purpose of passive control of duct noise, $L=50$ is too long. $L=10$ would be more practical. One may always design smaller channels (smaller $h^*$) so the dimensional length $L^*=h^*L$ may be limited. But for the same panel material and thickness, the dimensionless mass parameter, $M=M^*/\rho_0^* h^*$, becomes higher and the dimensionless frequency $f=f^*h^*/c_0^*$ of interest will be shifted towards the lower range. Our task now is to design a muffler which would give high transmission loss over the whole frequency range of $f\in(0,0.5)$. We compare the performance of the following two panel settings, the first being similar to the default:

(1) $M=10$, $L=10$, $\sigma=0.05$, $c_{T1}=1$, $c_{T2}=0.1$;
(2) $M=10$, $L=10$, $\sigma=0.15$, $c_{T1}=2$, $c_{T2}=0.025$.

The second setting has a higher loss factor and a larger range of thickness tapering, the results are shown in thick lines in Fig. 11 in the form of one-third octave averaging starting from a dimensionless center frequency of 0.0275. In general the highly tapered and damped panel experiences more sound reflection and less absorption except at very low and high frequencies. The example shows that, by appropriate adjustment, it is possible to have a rather good performance over the whole frequency range of plane waves. The performance shown here is comparable to that of a typical lined duct, cf. Beranek (1992), which gives somewhere between 3 dB and 4 dB attenuation per unit distance $h^*$ at the optimal frequency. At very low frequencies such as $f=0.0275$ (for a duct of 20 cm in height, $f^*=0.0275\times340/0.2=47$ Hz) lined ducts normally achieves some 0.6 dB per channel height using very resistive porous material, cf. Fig. 6.1.4 of Ingard (1994). Note that the latter is compiled for the single-sided duct lining, and the corresponding abscissa value of channel width/wavelength for the double lining channel should be $f/2=0.013\,75$. The TL reading of 0.3 dB is then doubled for the double lining. In our case the corresponding attenuation is 2 dB per $h^*$. This comparison means that a noise absorber

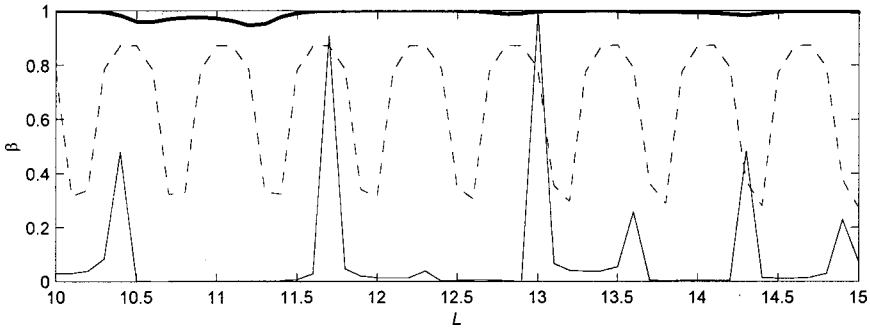


FIG. 10. Sound reflection on frictionless panels at frequency 0.15. The thick solid line is for the tapered panel showing near complete reflection for all length. The thin solid line is for the uniform panel of the same mass $M=10$ and tension. The dashed line is for much lighter uniform panels of $M=1$ and the same $c_T=0.2$.

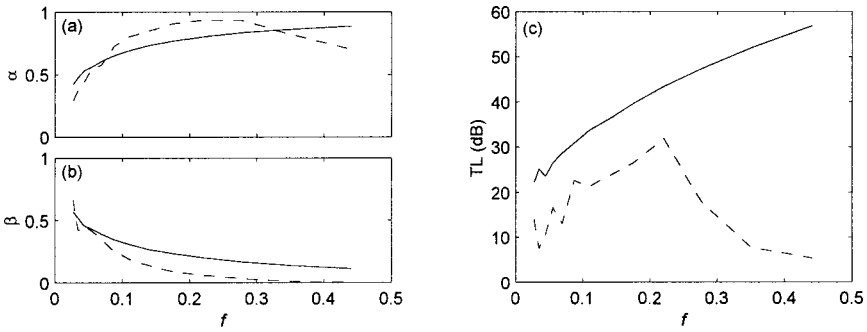


FIG. 11. Comparison of performance of panel muffler of length $L=10$ and $M=10$ in one-third octave band average starting from central frequency of 0.027 55. The thin lines have the default tapering setting of $c_{T1}=1$, $c_{T2}=0.1$, and $\sigma=0.05$, the thick lines are for $c_{T1}=2$, $c_{T2}=0.025$, $\sigma=0.15$.

made of tapered panel could achieve a transmission loss spectrum flatter than that of the conventional means.

## IV. CONCLUDING REMARKS

If a flexible panel is to be used as a muffler for passive noise control in a duct, it is desirable to have low reflection and high absorption. For energy absorption to be effective, sound must first be transferred from air to the flexural waves in structure. The energy transfer takes place when sound couples strongly with the wall vibrations, but significant sound reflection occurs near the panel leading edge if the coupling is spatially abrupt. To suppress such reflection, the phase speed of the coupled wave must approach the isentropic speed of sound in free space. But a perfect match is difficult to achieve at low frequencies since air imposes high virtual mass on the vibrating panel whose actual wave speed differs from its *in vacuo* value. Typically, sound energy is pumped into the structure near the leading edge and it gets absorbed by the internal friction of the panel as it travels downstream. The distribution of the local phase speed can be made to follow closely a decreasing *in vacuo* wave speed $c_T(x)$, which should have a smooth profile to avoid significant sound reflection along the length. Damping of flexural wave energy is enhanced by the slowing down of the waves. It may be said that similar idea of using tapered structure for energy damping was attempted in vibration isolation (Ungar and Kurzweil, 1984). The use of sound absorption wedges in anechoic chambers is another example of the same philosophy. A high degree of sound absorption may be achieved this way and the transmission loss spectrum can be rather flat for the whole frequency range of the fundamental duct acoustic mode. Although there are many realistic factors excluded from our theoretical modelling, the fact that such a flat spectrum is possible at all with tapered wall panels is an encouraging sign worthy of further studies.

If the tapered panel has no damping, however, sound reflection occurs all along the panel length. There is strong interference of reflection sound waves radiated by different parts of the panel, but the overall sound reflection can be much higher than that on a uniform panel. In addition, passband is effectively removed and this phenomenon alone is potentially useful in designing reactive muffler using tapered panels. One of the potential advantages of such a muffler is that it does not change the duct passage area, which means zero extra pressure loss.

## ACKNOWLEDGMENT

Funding support from the Research Grants Committee of the Hong Kong SAR and the Hong Kong Polytechnic University is gratefully acknowledged.

Ackermann, U., and Fuchs, H. V. (**1989**). ''Noise reduction in an exhaust stack of a papermill,'' Noise Control Eng. J. **33**, 57–60.

Ackermann, U., Fuchs, H. V., and Rambausek, N. (**1988**). ''Sound absorbers of a novel membrane construction,'' Appl. Acoust. **25**, 197–215.

Berry, B. S. (**1992**). ''Damping mechanisms in thin-layer materials,'' in *M3D: Mechanics and Mechanisms of Material Damping*, edited by V. K. Kinra and A. Wolfenden, ASTM STP 1169 (American Society for Testing and Materials, Philadelphia), pp. 28–44.

Beranek, L. L. (**1992**). *Noise and Vibration Control Engineering: Principles and Applications* (Wiley-Interscience, New York).

Cummings, A. (**1994**). ''Attenuation of sound in unlined ducts with flexible walls,'' J. Sound Vib. **174**, 433–450.

Doak, P. E. (**1973**). ''Excitation, transmission and radiation of sound from source distributions in hard-walled ducts of finite length (I): the effects of duct cross-section geometry and source distribution space-time pattern,'' J. Sound Vib. **31**, 1–72.

Ford, R. D., and McCormick, M. A. (**1969**). ''Panel sound absorbers,'' J. Sound Vib. **10**, 411–423.

Frommhold, W., Fuchs, H. V., and Sheng, S. (**1994**). ''Acoustic performance of membrane absorbers,'' J. Sound Vib. **170**, 621–636.

Huang, L. (**1999**). ''A theoretical study of duct noise control by flexible panels,'' J. Acoust. Soc. Am. **106**, 1801–1809.

Ingard, K. U. (**1994**). *Notes on Sound Absorption Technology* (Noise Control Foundation, New York).

Ungar, E. E. (**1997**). ''Vibration isolation and damping,'' *Handbook of Acoustics*, edited by M. J. Crocker (Wiley-Interscience, New York), Chap. 55.

Ungar, E. E., and Kurzweil, L. G. (**1984**). ''Structural damping potential of waveguide absorbers,'' in *Proceedings of Inter-Noise 84* (Noise Control Foundation, Poughkeepsie, New York, 1985), pp. 571–574.